Ultrafast far-infrared dynamics probed by terahertz pulses: a frequency domain approach. II. Applications

H. Němec, F. Kadlec, C. Kadlec, and P. Kužel*
Institute of Physics, Academy of Sciences of the Czech Republic, and Center for Complex Molecular Systems and Biomolecules Na Slovance 2, 182 21 Prague 8, Czech Republic

P. Jungwirth
Institute of Organic Chemistry and Biochemistry, Academy of Sciences of the Czech Republic, and Center for Complex Molecular Systems and Biomolecules Flemingovo nam. 2, 166 10 Prague 6, Czech Republic

We present data obtained by time-resolved terahertz spectroscopy in selected semiconducting and molecular systems exhibiting sub-picosecond far-infrared dynamics. We use a frequency-domain method which eliminates the influence of instrumental functions and artifacts due to frequency mixing and yields a two-dimensional transient conductivity of the photo-excited sample. This technique enables improving the attainable experimental time resolution and allows a simple qualitative interpretation of the results without a priori modeling. The quantitative interpretation is based on the time-dependent Drude and damped harmonic oscillators models.

I. INTRODUCTION

Optical pump—terahertz probe (OPTP) technique is a powerful experimental approach allowing one to access sub-picosecond to nanosecond dynamics of far-infrared (FIR) polar response. This is particularly due to the fact that the THz spectroscopy provides picosecond pulses of FIR radiation and that it can resolve the temporal profile of their electric field with a sub-picosecond resolution. On one hand the OPTP method proved to be able to bring valuable and new results in a large variety of physical and chemical systems: an excellent review has been published recently[1]. On the other hand, its methodology is still subject to development and improvement[2–5].

In the literature one can find three types of experimental works exploiting the OPTP technique. The most complete approach consists in an acquisition of a dense two-dimensional (2D) data grid in the time domain, i.e. in a measurement of a series of transient THz waveforms at closely spaced delays between the optical pump and the THz probe[6–13]. Strictly speaking, these 2D experimental data then should be treated *en bloc* to eliminate properly the instrumental functions and frequency mixing effects. This method then provides a complete picture of the ultrafast evolution of far-infrared polar spectra of photo-excited samples. The time resolution is limited by the length of the pump pulse and by the THz detection bandwidth. In the present paper we essentially deal with this type of experiments and, following Ref. 1, we refer to the method as to time-resolved THz spectroscopy (TRTS). In the second type of studies, the transient THz waveforms are obtained at a single or at several distinct (sparse) delays between the photo-excitation and the THz probing[14–17]. The individual transient waveforms are treated separately. The third approach consists in measurement of an effective transient THz response of the sample as a function of pump–probe delay. In these experiments a single point on the transient THz waveform or the integrated THz power are monitored during the variation of the pump–probe delay[15–24].

The last two approaches do not benefit from the excellent time resolution of the first one, rather they are limited by the length of the THz pulse[5]. Consequently, they can provide an equivalent amount of information only in the case of slow photo-induced processes, i.e. when the evolution of the system occurs on a timescale exceeding the THz pulse length. There are actually two main reasons why these simplified experimental approaches are used much more frequently than the first one: (i) a small magnitude of the signal in some systems so that complete 2D scans would be too noisy or time-consuming and (ii) a lack of methodology allowing a straightforward interpretation of 2D data without any *ad hoc* assumptions.

The first attempt to stress the importance and to clarify the TRTS measurement protocol has been made by Kindt and Schmuttenmaer[2]. Later on, two distinct methods have been proposed: (i) a numerical one based on finite-difference time-domain (FDTD) calculations[3,9] and (ii) an analytical one based on a 2D Fourier transformation[4]. The former approach has been applied by its authors to studyies of photo-carrier dynamics in semiconductors[9,10], of carrier transport in nanoparticles[12] and of environmental response in molecular systems[3,11]. The latter method has been further developed and supplemented by examples of theoretical modeling of dynamics in localized and delocalized states in the previous paper of this issue[5] (hereafter referred to as Paper I).

In the current paper we present TRTS experimental data obtained using the proposed experimental protocol for various systems of interest and we demonstrate the usefulness of this approach for their interpretation. Our aim is to provide a complete framework ready for direct application in experiments. Therefore we do not primar-

ily focus on physical interpretation of our results which are—at least in the case of semiconductor samples—to a large extent straightforward. Rather we stress the methodological aspects and the relevance of information obtainable by this experimental technique. Among the experimental works cited above there is a number of papers investigating FIR picosecond and sub-picosecond dynamics in technologically or scientifically interesting systems where the improved time resolution obtained by the application of our approach should bring new insight into the physics of the problem. In particular, this concerns experiments in microcrystalline silicon[22], in molecular crystals[23], in proton-bombarded InP[24] and in superconducting MgB_2[16].

The paper is organized as follows: in Sec. II we describe our experimental setup and protocols. Sec. III is devoted to TRTS characterization of radiation-damaged silicon-on-sapphire (RD-SOS) and Sec. IV deals with TRTS experiments in low-temperature grown GaAs (LT-GaAs). Finally, in Sec. V we work out and interpret our recently published data on the dynamics of 2,11,20,29-tetra-*tert*-butyl-2,3-naphthalocyanine (TBNC) in chloroform.

II. EXPERIMENTAL SETUP AND PROTOCOL

As a light source, we used a Quantronix Odin Ti:sapphire multi-pass femtosecond pulse amplifier producing ≈ 60 fs, 815 nm laser pulses with an energy about 1 mJ and a repetition rate 1 kHz. The pulses are split into three branches, all of them including delay lines for a precise control of pulse arrival times. One part of the laser output power is used for optically pumping the sample (pump branch). The second part of the pulses (probe branch) generates the THz probe radiation via optical rectification in a 1 mm thick [011] ZnTe crystal. The radiation is focussed onto the sample using an ellipsoidal mirror, leading to a peak electric field of the order of units of kV/cm. The third part of the pulses (sampling branch) is strongly attenuated and used for sampling the transmitted THz field using the electro-optic effect in another [011] ZnTe crystal.

A lock-in amplifier and a chopper operating at 166 Hz are used for the synchronous detection. The whole THz electric field intensity reaching the sensor can be acquired if the chopper is placed into the probe branch. This experiment is used as a reference (see below). If the chopper is moved into the pump branch, pump-induced changes in the THz waveform are detected (transient THz waveform). The performance of our setup for OPTP experiments has been discussed in Ref. 13.

A circular 3 mm diaphragm is placed behind the sample, so that the cross section of the excited volume (about 20 mm^2) is larger than that of the probed volume. In experiments with semiconductors we need rather low pump fluence to induce measurable changes in the FIR properties of the samples (typically $4 - 80$ $\mu J/cm^2$). Therefore we attenuate the pump beam using gray filters. We

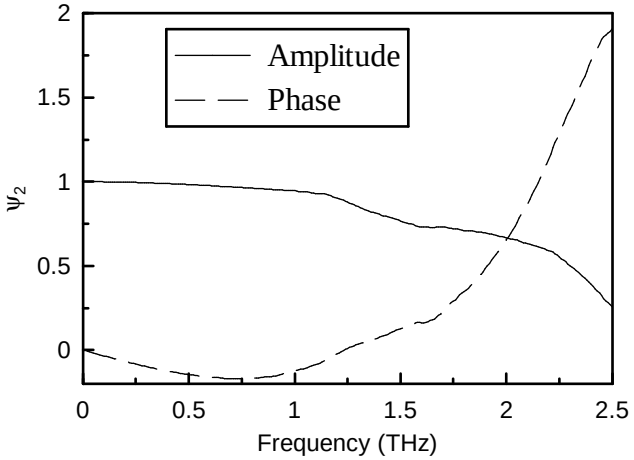

FIG. 1: Instrumental function of our ZnTe sensor.

can then use a dielectric-coated pellicle beam splitter to introduce the pump beam into the THz beam path and work in the collinear geometry. In contrast, we use a high pump fluence for experiments with TBNC (≈ 2 mJ/cm^2). In such conditions the pellicle beam splitter cannot be used: the angle of incidence of the pump pulse on the sample with respect to the direction of the probe pulse is about 10°. This might slightly distort the measured data, however, a comparison of our data with those in Ref. 11, where a collinear geometry was used, shows no quantitative difference.

A detailed discussion of the principle of measurements is presented in Paper I. The reader can find there (section II) the definitions of all experimental quantities used in the description below.

Prior to all measurements we have experimentally determined the instrumental function ψ_2 of our sensor (see Fig. 1)[25]. The majority of our experiments were performed in representation II (see Fig. 2a). A complete set of measurements for one sample then consists of four steps (the delay line D2 is held at a fixed position during all these steps). Note that the quantities accessed in individual steps can be identified with those expressed in Eqs. (5) and (12) in Paper I.

1. Output: reference measurement for the equilibrium transmission of the sample; positions A: empty diaphragm, B: sensor; pump beam: off; chopper: probe.

2. Output: $T(\omega)$, $\Xi^{(\mathrm{II})}(\omega, \omega - \omega_p)$, $E^D_{\mathrm{ref}}(\omega)$ (equilibrium properties of the sample and reference for 2D transient signal); positions A: sample, B: sensor; pump beam: off; chopper: probe.

3. Output: $\Delta E^{D,(\mathrm{II})}(\omega, \omega_p)$ (2D transient signal by scanning D1 and D3); positions A: sample, B: sensor; pump beam: on; chopper: pump.

4. Output: $E_0(\omega)$, $E_0(\omega - \omega_p)$ (waveform incident on the sample); positions A: sensor, B: not used; pump

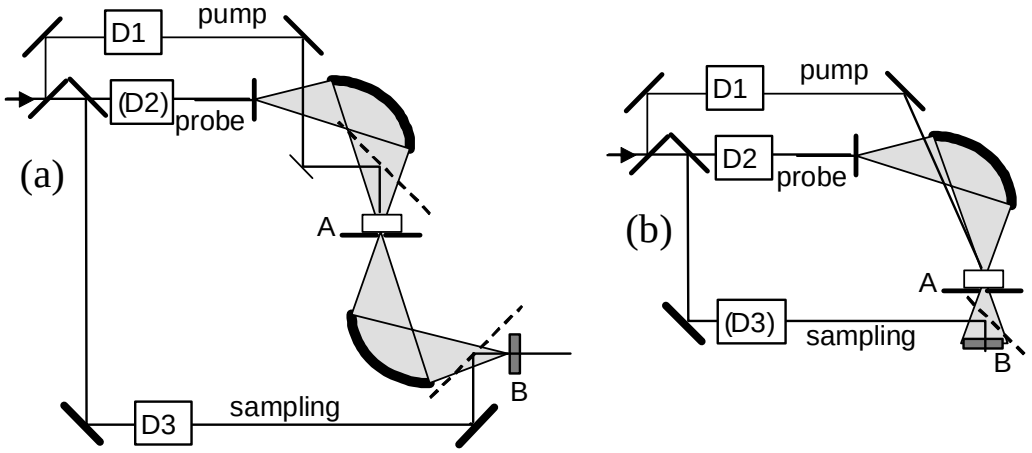

FIG. 2: Experimental setup. (a) Representation II, collinear pumping; (b) Representation I, noncollinear pumping.

beam: on (serves as a sampling beam; alternatively the pump beam can be cut and the sampling beam redirected to the pump beam path); chopper: probe.

The transient conductivity is then obtained from:

$$\Delta\sigma^{(\mathrm{II})}(\omega,\omega_p) = \frac{i\omega\epsilon_0 T(\omega)\ \Delta E^{D,(\mathrm{II})}(\omega,\omega_p)\ E_0(\omega)}{\Xi^{(\mathrm{II})}(\omega,\omega-\omega_p)\ E^D_{\mathrm{ref}}(\omega)\ E_0(\omega-\omega_p)}\,. \tag{1}$$

In all figures showing the transient conductivity spectra a dimensionless quantity $\Delta\sigma^{(\mathrm{II})}(\omega,\omega_p)/(2\pi\epsilon_0)$ is plotted.

In order to obtain the correct phase of $\Delta\sigma$ it is required to match appropriately the time origins of the signals obtained in steps 2 through 4. (i) The quantities $\Delta E^{D,(\mathrm{II})}$ and E^D_{ref} should have the same origin of the time delay τ, which is simply achieved by the fact the delay line D2 is fixed during all the steps. (ii) The quantity $\Delta E^{D,(\mathrm{II})}$ defines the origin of the pump–probe delay (τ_p), which corresponds to a specific overlapping position of the pump and probe at the sample input surface. The center of the pump pulse in this position thus defines the time origin which is to be taken for E_0. A precision of at least a few tens of fs can be reached if the pump beam is used for the sampling of the incident waveform as we propose in step 4 above. Otherwise, the origin of τ_p cannot be precisely experimentally obtained by other means and it should be taken as a variable parameter in subsequent fitting procedures.

The experiments with TBNC have been also performed in representation I (see Fig. 2b). In this case the delay line D3 is held in a fixed position. The transient THz signal should be measured in the far field without any beam transformation between the sample A and the sensor B. $T(\omega)$, $\Xi^{(\mathrm{I})}(\omega+\omega_e,\omega)$ are already known and the knowledge of the waveform incident on the sample is not required. Two steps are performed:

1. Output: $E^D_{\mathrm{ref}}(\omega)$ (reference for 2D transient signal); pump beam: off; chopper: probe.
2. Output: $\Delta E^{(\mathrm{I})}(\omega,\omega_e)$ (2D transient signal by scanning D1 and D2); pump beam: on; chopper: pump.

A complete experiment on one sample is rather long. Typically, our experiments on semiconductors take about 3 hours and the experiments on TBNC last about 4–5 hours. The experimentalist then should ensure a very good power stability and especially the beam-pointing stability of the laser system during the whole set of measurements. For example, errors in the reference measurements can lead to significant errors in the output data. Following our experience it is usually worth to perform the experiment twice on one sample—this provides a good check of the correctness of all the data.

III. ULTRAFAST DYNAMICS IN RD-SOS

The RD-SOS is a material exhibiting a short carrier lifetime τ_c which is owing to the fast carrier trapping on deep levels created by ion implantation in the silicon lattice. The response time of the semiconductor can reach sub-picosecond values[26,27] and depends on the implantation dosage and on ion energies that are used for the sample preparation. At the same time, the velocity scattering time τ_s is of about 50 fs or shorter[20,27,28]. It then appears rather challenging to test the time resolution of OPTP experiments carried out with the use of our methodology on such samples with very short characteristic times.

In the experiments we used two 1μm thick independently prepared samples (denoted as #1 and #2) selected to exhibit very fast time responses. The irradiation doses were approximately 10^{14} cm^{-2} using 100 keV O^+ ions. The pump-beam fluence used in the experiment was ≈ 80 μJ/cm^2. We verified that this fluence did not lead to non-linear phenomena like trap filling: the transient signal scaled linearly with the pump fluence when neutral density filters were inserted into the pump-beam path. At the same time, the signal was sufficiently small

to enable the use of the weak-signal limit specified in Paper I. The sapphire substrate is transparent for the pump beam and cannot contribute to the transient signal. Representation II was used. The temporal area scanned by τ and τ_p delays was rectangular with side lengths 12.7 ps and 6.3 ps and the entire rectangle was covered using 100 fs steps for both delays (128×64 points).

The whole data set obtained allows us to apply a complete 2D data treatment as it has been described in Paper I. For illustration and also for comparison with our methodology, we analyze in addition some particular one-dimensional (1D) scans (pump–probe scans or waveform scans).

Figs. 3 (for sample #1) and 4 (for sample #2) show the 2D spectra of the complex conductivity $\Delta\sigma(\omega,\omega_p)$ calculated from the measured data using Eq. (1). For this calculation, the transfer function $\Xi(\omega,\omega-\omega_p)$ was determined using the equilibrium characteristics of the sample (Fig. 5). Note that in this case Ξ virtually does not depend on ω_p and that, in the first order of development, for strongly absorbing samples $\Xi \propto i\omega$ [cf. expression (7) in Paper I].

The amplitude spectrum of the conductivity for both samples shows a behavior characteristic for the dynamics of free carriers (refer also to Fig. 2 in Paper I). The decrease of the amplitude with frequency ω_p indicates that the carrier trapping time τ_c falls on the time scale of hundreds of femtoseconds. In contrast, the flatness of the spectrum in the ω-direction suggests very fast momentum scattering rates of the electrons (τ_s < 50 fs).

A complex fitting with a Drude model has been performed minimizing the function

$$\sum_{\omega,\omega_p} \left|\Delta\sigma_{\mathrm{exp}}(\omega,\omega_p) - \Delta\sigma_{\mathrm{Drude}}(\omega,\omega_p)\right|^2 , \qquad (2)$$

where[5]

$$\Delta\sigma_{\mathrm{Drude}}(\omega,\omega_p) = \frac{e^2 n_0}{m^*}\,\frac{1}{i\omega + 1/\tau_c + 1/\tau_s}\,\frac{1}{i\omega_p + 1/\tau_c} , \qquad (3)$$

and where n_0 is the free electron density and $m^* \approx 0.26\ m_e$ is the electron mass in the conduction band of Si. Let us emphasize that the fit can be performed in two manners. (i) The amplitude factor of the transient conductivity can be considered as an unknown fitting parameter (fit with variable amplitude factor): in this case the momentum scattering time appears too short (< 50 fs) and cannot be precisely determined from the fit due to the upper-frequency detection limit of our sensor. (ii) The amplitude factor can be fixed to an estimated value of the free electron density determined from the absorption coefficient of Si at 800 nm and from the incident pump fluence ($n_0 \approx 3.2 \times 10^{17}$ cm^{-3}). In this case even extremely short momentum scattering times can be evaluated from the experiment. The results of such fits are shown in Fig. 3 for sample #1. In addition, we show the amplitude of the complex residuals of the fit for sample #2 (Fig. 4). The Drude model fits the measured conductivity quite well: the spectrum of residuals appears close to the white noise. The values of fitting parameters are summarized in Table I. The values of the trapping times appear to be somewhat shorter than those found in Ref. 26 and significantly shorter than those reported in Ref. 27. This can be related to the different pump wavelength used in these experiments: the use of 625 nm in Ref. 26 (or even 400 nm as in Ref. 27) implies a non-vanishing population of free electrons in the L-valley and should lead to different carrier scattering mechanisms.

For comparison we show below a partial analysis of our experimental data by treating individual scans. Fig. 6 shows the waveform $E_0(t)$ incident on the sample and several examples of pump–probe scans. It contains experimental data for sample #1 in which a single point on the THz waveform ($\tau = \tau_0$) is monitored during the variation of the pump–probe delay (τ_p). The corresponding points at the incident THz waveform (τ_0) are shown in the inset. Within a simplified approach one would obviously try to fit this kind of curves by a single exponential decay. Clearly, some of the pump–probe scans are not convenient for such fitting (e.g. the dashed line in Fig. 6). In other cases, the fitting is possible, however, the fitting range for the exponential can be chosen to some extent arbitrarily and its choice influences the resulting decay constant. For the present data, where the transient waveform is approximately out-of-phase with respect to the incident waveform, the fitting appears to be most reliable close to the maximum and minimum of the incident waveform. We performed a series of such fits for pump–probe scans with τ_0 ranging from -0.2 to 0 ps and from 0.2 to 0.4 ps (these ranges correspond to the gray areas in the inset). The decay rates obtained by the fits span over the range 320–470 fs (with an average value of 415 fs) for sample #1 and over the range 380–570 fs (with an average value of 500 fs) for sample #2.

In conclusion, in this particular case the average values obtained by 1D fitting correspond quite well to the results obtained using our methodology (cf. Table I). However, results of the fitting of individual scans depend on the fitting range and display a significant spread. In this respect the 2D approach is unambiguous and straightforward.

Fig. 7 contains transient THz spectra as calculated by a simple 1D Fourier transformation from the measured data, i.e., $\Delta E^D(\omega,\tau_p)/E^D_{\mathrm{ref}}(\omega)$ is plotted for several pump–probe delays. Note that the spectra obtained using this (oversimplified) procedure apparently do not resemble to simple Drude-like spectra despite of the fact that we demonstrated above that free carriers do follow the Drude dynamics in our experiments. Namely, considering only these spectra, one could (incorrectly) infer a departure from a Drude-like behavior of the carriers at early times after photo-excitation. These features occurring in the transient THz spectra have been discussed in detail in Paper I: see Eq. (40) and Fig. 4 therein. They are a consequence of the frequency mixing during ultra-

fast time evolution of the system studied. Notice, in Fig. 7, that the experimental data are in a good agreement with the lines which are based on Eq. (40) in Paper I including the Drude model and taking inherently into account the frequency mixing.

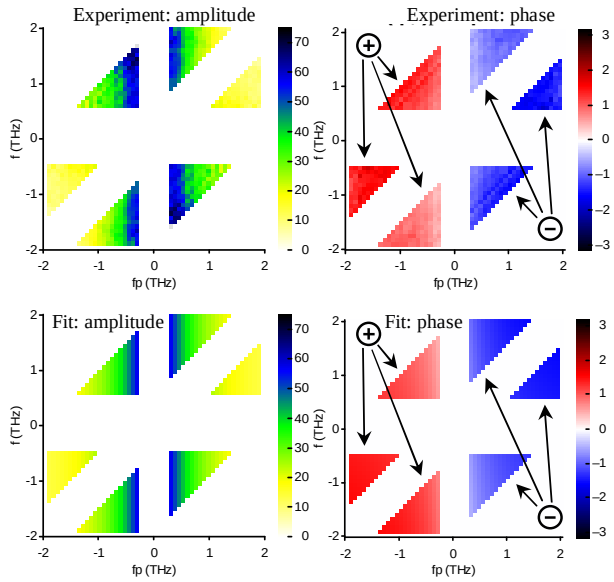

FIG. 3: Amplitude and phase of the 2D conductivity $\Delta\sigma(\omega,\omega_p)/\epsilon_0$ of RD-SOS (sample #1). Upper row: experiment, lower row: best fit to the Drude model.

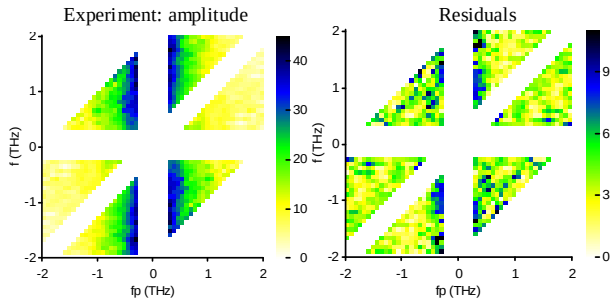

FIG. 4: Left part: Amplitude of the complex conductivity $\Delta\sigma(\omega,\omega_p)$ of RD-SOS (sample #2). Right part: residuals of the complex fit using Drude model, $|\Delta\sigma_{\rm exp}(\omega,\omega_p) - \Delta\sigma_{\rm Drude}(\omega,\omega_p)|$.

IV. ULTRAFAST DYNAMICS IN LT GAAS

Low-temperature (LT) grown GaAs is grown by molecular beam epitaxy at temperatures lower than 300 K. The deposition conditions allow for the forming of a large concentration of ionized arsenic antisite defects which act as deep and efficient electron traps.[15,29] The investigated samples consisted of a semi-insulating GaAs substrate covered by a 100 nm GaAs buffer layer deposited

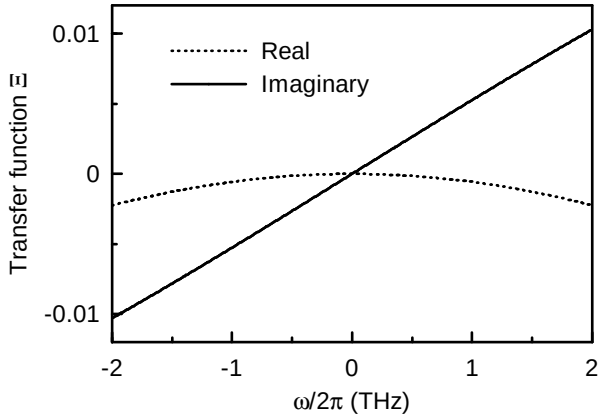

FIG. 5: Transfer function $\Xi(\omega,\omega-\omega_p)$ for RD-SOS samples. The function is practically independent of ω_p.

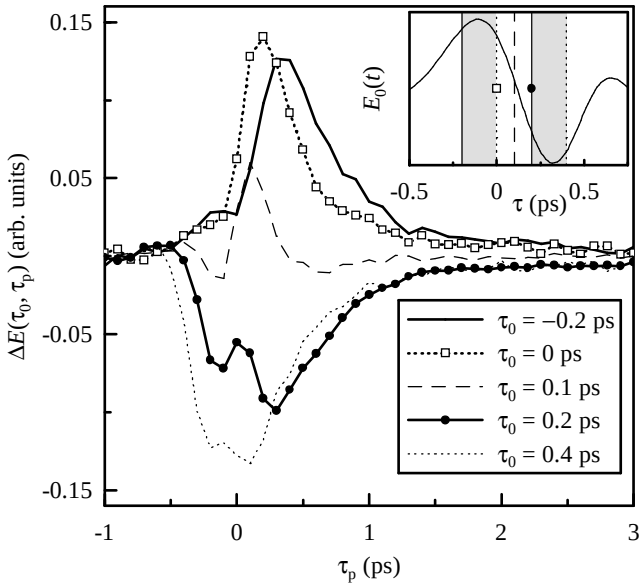

FIG. 6: Transient THz signal obtained for RD-SOS (sample #1) representing 1D pump–probe scans at a fixed waveform position ($\tau=\tau_0$). Inset: shape of the THz incident waveform as measured using our ZnTe sensor. The lines correspond to different waveform positions (τ_0) indicated in the inset: the motifs of lines (and points) mutually correspond.

at 590 °C and by a 2.5 μm thick layer grown at temperatures 200 (sample #958) or 250 °C (sample #959). Both samples were subsequently annealed for 10 min at 600°C in order to restore a high electron mobility.[30]

The experiments were performed using representation II. The pump-beam fluences ranged between 2 and 4 μJ/cm^2. Such fluences yield a THz transient signal of the order of units of per cent of the incident field strength and do not lead to the trap filling phenomena. In contrast with the sapphire substrate, the semi-insulating GaAs substrate used in this study contributes to the transient signal by a long-lived decay. This is due to the fact that about 5 % of the pump power is absorbed in the sub-

TABLE I: Values of the fitting parameters for semiconducting samples

	Amplitude variable (fitted)			Amplitude fixed by n_0		
Sample	τ_c (ps)	τ_s (fs)	μ ($\mathrm{cm^2V^{-1}s^{-1}}$)	n_0 ($\mathrm{cm^{-3}}$)	τ_s (fs)	μ ($\mathrm{cm^2V^{-1}s^{-1}}$)
RD-SOS #1	0.55	< 50	< 340	3.2×10^{17}	25	160
RD-SOS #2	0.42	< 50	< 340	3.2×10^{17}	35	240
LT GaAs #959	1.9	< 50	< 1300	0.44×10^{17}	30	800
LT GaAs #958	1.1	< 50	< 1300	1.1×10^{17}	45	1200

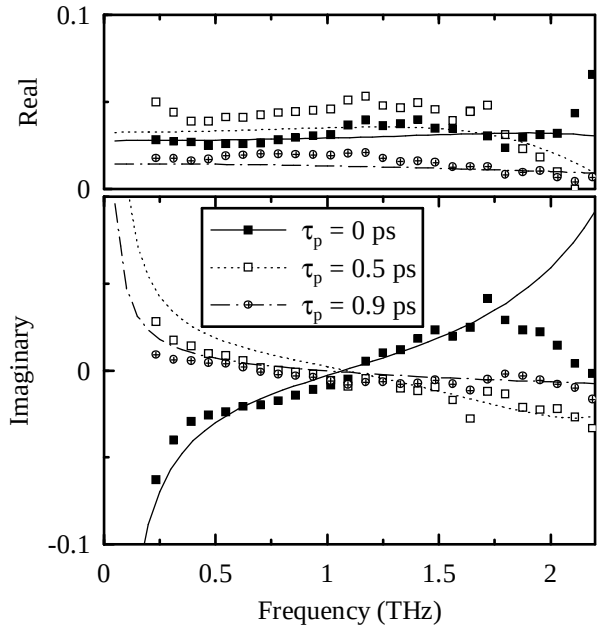

FIG. 7: 1D Fourier transformation of the transient waveforms obtained for RD-SOS (sample #1) for different pump–probe delays (τ_p). Points: experimental data obtained as $\Delta E^D(\omega, \tau_p)/E^D_{\mathrm{ref}}(\omega)$; lines: simulations of the measured data using the model developed in Paper I (parameters: $\tau_s = 0.035$ ps, τ_c= 0.42 ps) and using a numerical approximation of the incident THz waveform.

strate.

On one hand, the LT grown layers studied exhibit carrier lifetimes in the range 1–2 ps, which is comparable or even slightly longer than the THz pulse length. This means that the dynamical properties of these samples are very close to (or even within) the limits where the transient signal can be treated by means of 1D transient waveforms and/or 1D pump–probe scans without any loss of information. The results we obtain using our methodology thus can be easily checked. On the other hand, the system is expected to show an additional long-lived component due to the much slower carrier recombination in the bulk substrate. In the Fourier space, such a slow component leads to a marked narrow peak with broad wings superimposed over the signal coming from the LT layer. These two signals have comparable magnitudes, which means that small errors in the slow component may lead, in the frequency domain, to a significant uncertainty in the parameters describing the fast component. In this sense, the application of our methodology to these samples is expected to be difficult. Testing of our methodology is the primary reason of our choice of this system.

The slow component related to the bulk substrate can be in principle subtracted from the measured signal. Using very long 1D pump–probe scans it is possible to determine the dynamical parameters of the bulk GaAs. In our case, we obtain $\tau_{c,\mathrm{bulk}} = 106$ ps for the carrier lifetime. For the bulk momentum scattering time we used the value from the literature[31]: $\tau_{s,\mathrm{bulk}} = 270$ ps. Using two different experimental approaches it is possible to subtract the signal related to the bulk substrate either in the frequency domain by fitting of the transient conductivity or directly in the time domain from the raw data. The former method is applied in case of sample #958, the latter one is demonstrated for sample #959.

With the sample #958, a rectangular temporal area 10 ps × 10 ps in τ and τ_p was scanned. The waveforms obtained for long pump–probe delays $\tau_p \geq 8$ ps do not change their shape any more when τ_p is gradually increased; they only scale in a linear way since the dynamics of the signal is completely described by the slow decay related to the bulk GaAs. This allows us to calculate waveforms for longer pump–probe delays using the experimentally determined value of $\tau_{c,\mathrm{bulk}}$. In this way we have obtained a rectangular data area with side lengths 10 ps and 300 ps. It is important to stress that in this case the subtraction of the signal coming from the substrate must be performed in the frequency domain after appropriate deconvolutions described by Eq. (1). The reason is that a successful simulation of experimental data in the time domain for early pump–probe delays would in fact require an exact knowledge of all the instrumental functions. By contrast, it is possible to simulate the transient conductivity response of the substrate in the frequency domain using the values of the parameters $\tau_{c,\mathrm{bulk}}$ and $\tau_{s,\mathrm{bulk}}$ and the known value of the fluence absorbed in the substrate.

The upper row of Fig. 8 shows the measured amplitude spectrum of the transient conductivity and a fit by two Drude terms analogous to that defined by Eq. 3. One term is related to the LT grown layer (its parameters are variable) and the other one describes the bulk substrate (its parameters are fixed to the known values). Note that for this sample the transient conductivity for $\omega, \omega_p < 0.4$ THz is not shown in Fig. 8 and was not taken into account in the fits. This is because in this part of the

spectrum the signal is dominated by the slow contribution coming from the substrate. Consequently, relatively small errors in the modeling of the substrate properties could significantly change the fitting parameters of the LT layer.

For sample #959, we scanned a rectangular temporal area 10 ps × 12 ps in τ and τ_p first in an arrangement where the LT layer faces the pump beam. Subsequently, we turned the sample and repeated the whole experiment with the LT layer turned away from the pump which yields the pure substrate response. The difference of these 2D signals was calculated directly in the time domain using an appropriate amplitude scaling. The 2D transient conductivity related to the dynamics of the LT layer only was then obtained from this difference signal and is shown in the lower row of Fig. 8. Finally, it was fitted to the Drude model following the procedure described in section III. The resulting parameters are shown in Table I. The obtained carrier lifetimes are in agreement with those obtained by 1D pump–probe scans.

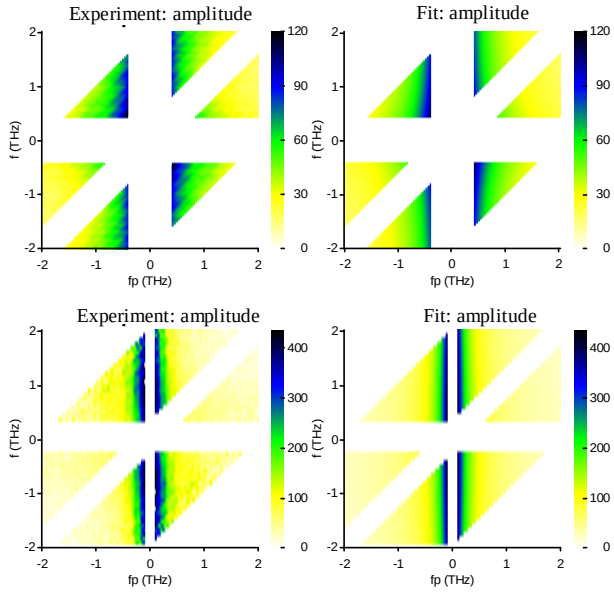

FIG. 8: Amplitude of the 2D conductivity $\Delta\sigma(\omega,\omega_p)$ of LT GaAs samples: measured spectra (left part) and the fits (right part), see the text for details. Upper row: sample #958, lower row: sample #959.

V. ULTRAFAST DYNAMICS IN TBNC

During last years a considerable experimental effort has been made to understand the dynamics of solute–solvent interaction in polar solutions. The solvent relaxation following photo-excitation of the solute influences a large number of chemical processes. Recently, experimental OPTP data were obtained for TBNC in polar solvents (e.g. chloroform)[11,13]. The experimental data were most recently interpreted as coming from a polycrystalline phase which is formed in the solution upon strong photo-excitation[13]. In this paragraph we analyze the raw experimental data we have presented in Ref. 13. To illustrate our methodology for this case, we performed experiments in both representations (i.e. using both experimental schemes of Fig. 2). Concerning representation I, in the first step, the conductivity $\Delta\sigma^{\mathrm{I}}(\omega,\omega_e)$ was directly obtained from the experimental data measured in an arrangement according to Fig. 2b. In the second step, this function was transformed to representation II using the transformation $\Delta\sigma^{(\mathrm{I})}(\omega,\omega_e)=\Delta\sigma^{(\mathrm{II})}(\omega+\omega_e\rightarrow\omega,\omega_e\rightarrow\omega_p)$. The signal-to-noise ratio of these data is rather poor because the focusing of the transient THz signal is not allowed for this arrangement. For this reason, only spectra obtained directly in representation II were used for fitting. Fig. 9 shows the transfer function Ξ for the TBNC in chloroform enclosed in an infrasil cuvette and Figs. 10a,b show experimental results for the transient conductivity obtained using both representations. Both figures are in a semi-quantitative agreement (note that the phase should be compared only in the regions where the amplitude significantly exceeds the noise level). Their major common feature is a broad pole at $\omega/2\pi\approx 1.2$ THz and $\omega_p\approx 0$, in a sharp contrast with the results obtained in the case of semiconductors. The observed behavior in TBNC is characteristic for a damped localized-state dynamics (see Paper I). Let us emphasize that so far we have not used any assumption about the system under investigation. Our methodology thus allows a simple and unambiguous recognizing between the dynamics in a localized or delocalized state from the conductivity amplitude profile.

We studied the results shown in Fig. 10 using the model for excitation of a damped vibrational mode in a harmonic approximation described in Paper I [Eqs. (47) and/or (48)]. Some qualitative conclusions can be made by simple comparing of the experimental 2D complex spectra with simulated ones based on the existence of the above mentioned pole at 1.2 THz. (i) The pole is related to the excited-state dynamics, i.e., ω_E, and not to ω_G (see simulations of the conductivity phase in Figs. 10e,f); (ii) the observed dynamics is described by a strongly perturbed system rather than a weakly perturbed one (see simulations of the conductivity amplitude in Figs. 10c,d). Let us recall that in strongly coupled systems (described by Eq. (47) in paper I) the THz motion in the excited state is unrelated to that in the ground state (i.e. the actual velocities and positions of the particles are averaged during photo-excitation event).

The fitting of the complex spectra then yields the following parameters (Fig. 10c): frequency of the excited state $\omega_E/2\pi = 1.2$ THz, damping in the excited state $\gamma_E \approx 3$ ps^{-1}, excited state population relaxation time $\tau_c \approx 0.9$ ps, frequency of the ground state $\omega_G/2\pi \gtrsim 2$ THz, the mode is overdamped ($\gamma_G \gtrsim 10$ ps^{-1}).

The first attempt of a quantitative interpretation of the dynamics of the system TBNC/chloroform was made by Beard et al.[11] who described the system using a

model equivalent to our harmonic oscillator model in the strongly perturbed limit. The authors naturally assumed that the far-infrared dynamics was closely related to the motion of the chloroform molecules solvating the dye. Based on these assumptions they identified the ground-state parameters of OPTP experiments with those $(\omega_{\rm chl}, \gamma_{\rm chl})$ obtained from the equilibrium THz spectrum of chloroform, i.e., $\omega_G/2\pi = \omega_{\rm chl}/2\pi \approx 1.2$ THz and $\gamma_G = \gamma_{\rm chl} \approx 5$ ps^{-1}. In the next step, the authors simulated their time-domain experimental data using an overdamped oscillator representing the excited state ($\omega_E/2\pi \approx 3$ THz) and with $\tau_c \approx 1.4$ ps.

It follows from more recent experiments[13] that the observed transient dynamics is apparently connected to the existence of a solid polycrystalline phase of TBNC in the solution. The experimental results were then proposed to be interpreted in the framework of transient phonon spectra in solid TBNC. Nevertheless, the coincidence of the equilibrium eigen-frequency of chloroform $\omega_{\rm chl}$ and the OPTP excited-state frequency ω_E is striking. Note also the similarity of the numerical values of all the parameters obtained in the present study with those found in Ref. 11 provided, however, that the significance of the ground and excited state is reversed. One cannot thus completely exclude a hypothesis that the observed phenomena are related to the interface between the solid phase and the solution (note that the transient signal has never been observed in our experiment without the presence of the solid phase). Within such a hypothesis the ground state of the system would be assigned to a specific state of the interface (with some concentration of chloroform molecules bound to the surface). The photo-excitation then would be connected to the detachment of these molecules: this mechanism provides a connection between the equilibrium motion characterized by $\omega_{\rm eq}$ and ω_E. Note, however, that the photo-excitation of the molecular crystal of TBNC has a local character and an analogous frequency change is not observed for individual solvated molecules of TBNC. The physical process which could lead to such a qualitative difference is not clear. In addition, in such a case, the measured signal would have to arise from a single layer located at the interface. However, this contribution is expected to be negligible compared to that coming from the bulk. The interpretation that the transient signal comes from the bulk of the crystalline phase of TBNC and is not in a direct relationship with the properties of the solvent thus seems to be most plausible in the current state of understanding of the problem.

VI. CONCLUSION

We applied a frequency domain methodology of the optical pump—THz probe experiments to two ultrafast semiconductor systems (RD-SOS and LT GaAs on semi-insulating GaAs substrate) and to a molecular system of TBNC in chloroform. The observed ultrafast dynamics was interpreted in terms of two-dimensional complex transient conductivity. We showed in detail how to use this method for investigation of sub-picosecond far-infrared dynamics and demonstrated its advantages over one-dimensional pump–probe or transient waveform approaches.

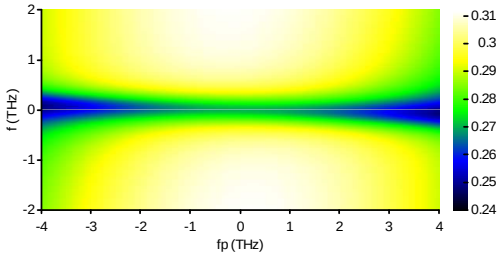

FIG. 9: Amplitude of the transfer function $|2\pi\Xi(\omega, \omega - \omega_p)/i\omega|$ for TBNC in chloroform used in the calculations.

These systems illustrate the general features of our methodology. The 2D transient conductivity spectra are obtained directly without any modeling and they allow a straightforward qualitative judgment about the character of the observed dynamics (localized versus delocalized state dynamics). Subsequent modeling and complex fitting of the spectra allows for reliable determination of the model parameters. In the case of free carrier dynamics, both carrier trapping time and momentum scattering time can be determined with a resolution of about 100 fs or better. For bound charges, it is important to carefully analyze the information contained in both amplitude and phase spectra in order to understand the underlying charge dynamics.

Acknowledgments

We are thankful to P. Mounaix, L. Duvillaret and W. Hansen for providing semiconductor samples. The financial support from the Ministry of Education of the Czech Republic (project No. LN00A032) is gratefully acknowledged.

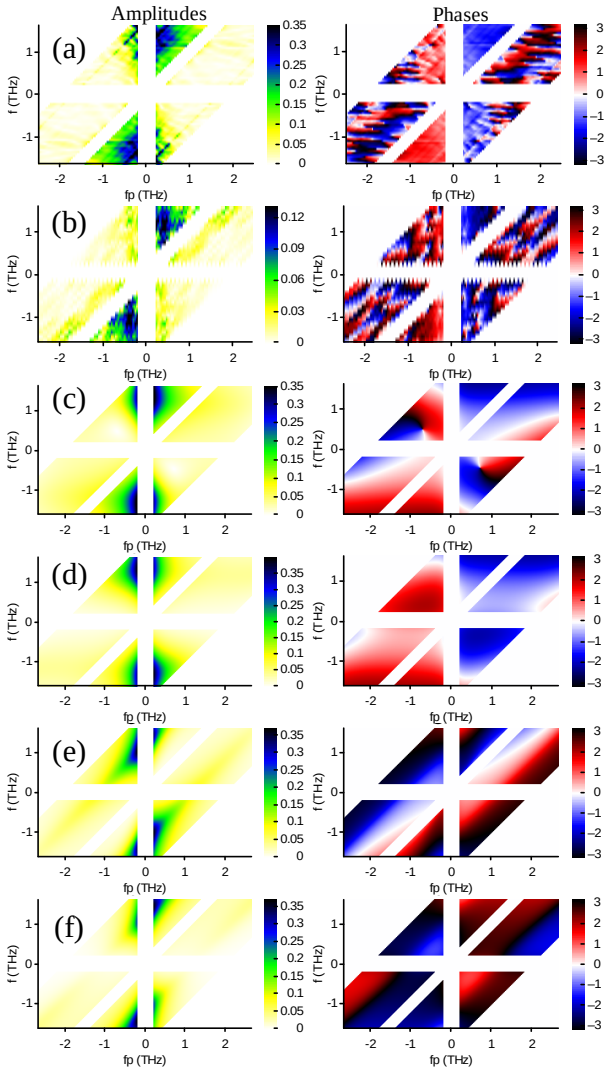

FIG. 10: Amplitude and phase of the transient conductivity $\Delta\sigma^{\mathrm{II}}(\omega,\omega_p)$ of TBNC in chloroform. (a) and (b) Experimental results obtained using the arrangement shown in Fig. 2a and b, respectively. (c)–(f) Simulations using a damped harmonic oscillator model; $\omega_1/2\pi = 1.2$ THz, $\omega_2/2\pi = 2.2$ THz, $\gamma_1 = 3$ ps^{-1}, $\gamma_2 = 11$ ps^{-1}, $\tau_c = 0.88$ ps in all cases. (c) strong perturbation limit, $\omega_E = \omega_1$, $\gamma_E = \gamma_1$, $\omega_G = \omega_2$, $\gamma_G = \gamma_2$. (d) weak perturbation limit, same parameters as in (c). (e) strong perturbation limit, $\omega_E = \omega_2$, $\gamma_E = \gamma_2$, $\omega_G = \omega_1$, $\gamma_G = \gamma_1$. (f) weak perturbation limit, same parameters as in (e).

* Electronic address: kuzelp@fzu.cz

[1] C. A. Schmuttenmaer, Chem. Rev. **104**, 1759 (2004).
[2] J. T. Kindt and C. A. Schmuttenmaer, J. Chem. Phys. **110**, 8589 (1999).
[3] M. C. Beard and C. A. Schmuttenmaer, J. Chem. Phys. **114**, 2903 (2001).
[4] H. Němec, F. Kadlec, and P. Kužel, J. Chem. Phys. **117**, 8454 (2002).
[5] H. Němec, F. Kadlec, S. Surendran, P. Kužel, and P. Jungwirth, J. Chem. Phys. (2004), previous paper in this issue.
[6] J. Zielbauer and M. Wegener, Appl. Phys. Lett. **68**, 1223 (1996).
[7] R. Huber, F. Tauser, A. Brodschelm, M. Bichler, G. Abstreiter, and A. Leitenstorfer, Nature **414**, 286 (2001).
[8] R. A. Kaindl, M. A. Carnahan, D. Hägele, R. Lövenich, and D. S. Chemla, Nature **423**, 734 (2003).
[9] M. C. Beard, G. M. Turner, and C. A. Schmuttenmaer, Phys. Rev. B **62**, 15764 (2000).

[10] M. C. Beard, G. M. Turner, and C. A. Schmuttenmaer, J. Appl. Phys. **90**, 5915 (2001).
[11] M. C. Beard, G. M. Turner, and C. A. Schmuttenmaer, ACS Symposium Series 820 (ACS, Washington DC, 2002).
[12] G. M. Turner, M. C. Beard, and C. A. Schmuttenmaer, J. Phys. Chem. B **106**, 11716 (2002).
[13] F. Kadlec, C. Kadlec, P. Kužel, P. Slavíček, and P. Jungwirth, J. Chem. Phys. **120**, 912 (2004).
[14] R. D. Averitt, G. Rodriguez, J. L. W. Siders, S. A. Trugman, and A. J. Taylor, J. Opt. Soc. Am. B **17**, 327 (2000).
[15] S. S. Prabhu, S. E. Ralph, M. R. Melloch, and E. S. Harmon, Appl. Phys. Lett. **70**, 2419 (1997).
[16] J. Demsar, R. D. Averitt, A. J. Taylor, V. V. Kabanov, W. N. Kang, H. J. Kim, E. Choi, and S. Lee, Phys. Rev. Lett. **91**, 267002 (2003).
[17] P. N. Saeta, J. F. Federici, B. I. Greene, and D. R. Dykaar, Appl. Phys. Lett. **60**, 1477 (1992).
[18] G. Haran, W.-D. Sun, K. Wynne, and R. M. Hochstrasser, Chem. Phys. Lett. **274**, 365 (1997).
[19] R. McElroy and K. Wynne, Phys. Rev. Lett. **79**, 3078 (1997).
[20] K. P. H. Lui and F. A. Hegmann, Appl. Phys. Lett. **78**, 3478 (2001).
[21] E. Knoesel, M. Bonn, J. Shan, and T. F. Heinz, Phys. Rev. Lett. **86**, 340 (2001).
[22] P. Jepsen, W. Schairer, I. Libon, U. Lemmer, N. Hecker, M.Birkholz, K. Lips, and M. Schall, Appl. Phys. Lett. **79**, 1291 (2001).
[23] F. A. Hegman, R. R. Tykwinsky, K. P. H. Lui, J. E. Bullock, and J. E. Anthony, Phys. Rev. Lett. **89**, 227403 (2002).
[24] C. Messner, H. Kostner, R. A. Höpfel, and K. Unterrainer, J. Opt. Soc. Am. B **18**, 1369 (2001).
[25] H. J. Bakker, G. C. Cho, H. Kurz, Q. Wu, and X.-C. Zhang, J. Opt. Soc. Am. B **15**, 1795 (1998).
[26] F. E. Doany, D. Grischkowsky, and C.-C. Chi, Appl. Phys. Lett. **80**, 460 (1987).
[27] K. P. H. Lui and F. A. Hegmann, J. Appl. Phys. **93**, 9012 (2003).
[28] P. R. Smith, D. H. Auston, A. M. Johnson, and W. M. Augustyniak, Appl. Phys. Lett. **38**, 47 (1981).
[29] S. Gupta, J. F. Whitaker, and G. A. Mourou, IEEE J. Quantum Electron. **28**, 2464 (1992).
[30] J. K. Luo, H. Thomas, D. V. Morgan, and D. Westwood, J. Appl. Phys. **79**, 3622 (1996).
[31] S. M.Sze, *Semiconductor devices* (Wiley, New York, 1985).